

Dielectric Permittivity Estimation via TDR Measurements

*Original*

Dielectric Permittivity Estimation via TDR Measurements / Nakano, M. S.; Savi, P.. - ELETTRONICO. - (2009), pp. 921-924. ( International Conference on Electromagnetics in Advanced Applications (ICEAA 09) Torino (Italy) September, 14-18, 2009) [10.1109/ICEAA.2009.5297327].

*Availability:*

This version is available at: 11583/2373038 since: 2022-01-26T22:48:09Z

*Publisher:*

IEEE

*Published*

DOI:10.1109/ICEAA.2009.5297327

*Terms of use:*

This article is made available under terms and conditions as specified in the corresponding bibliographic description in the repository

*Publisher copyright*

IEEE postprint/Author's Accepted Manuscript

©2009 IEEE. Personal use of this material is permitted. Permission from IEEE must be obtained for all other uses, in any current or future media, including reprinting/republishing this material for advertising or promotional purposes, creating new collecting works, for resale or lists, or reuse of any copyrighted component of this work in other works.

(Article begins on next page)

# Dielectric Permittivity Estimation via TDR Measurements

M. Satoru Nakano\*

P. Savi\*

**Abstract** — In this paper the determination of the permittivity of liquid or homogeneous dielectrics from their time-domain response is addressed. The analysis is based on a simplified model of the TDR measurement setup, where the probe is described by an ideal transmission line with a Debye permittivity. A simple formula to evaluate the permittivity is introduced, and compared with other well-known methods for the permittivity determination based on the calculation of the travel time of the TDR signal along the probe.

## 1 INTRODUCTION

Time-Domain Reflectometry (TDR) has been widely applied in soil science, hydrology and agronomy to estimate the permittivity of soils [1; 2]. Owing to this application, over the past 20 years, great efforts have been spent on the modeling of TDR measurement systems and on the methods to solve the inverse problem of estimating the permittivity from the reflection responses. The two major features of TDR waveforms are the travel time in the probe and the long time amplitude of the response, that are directly related to the apparent dielectric dielectric constant and to the soil electrical conductivity.

Several studies in the literature have aimed at determining a good method to evaluate the travel time from the TDR curve [3; 4]. In order to overcome the difficulties in the determination of the starting and ending point of this time interval, in this paper, an ideal model of the measurements setup and a frequency domain analysis leading simple relations to evaluate the permittivity are introduced.

## 2 ANALYSIS

In order to analyse the TDR response, we consider the simplified model of the TDR measurement system shown in Fig. 1 where an ideal voltage step (infinite bandwidth) is applied to an ideal cable of characteristic admittance  $Y_o$  connected to the probe. The probe is an open-ended ideal coaxial line and can be modeled as a TEM transmission line of characteristic admittance and time delay of the empty line  $Y_a$  and  $\tau_a$ , respectively [5]. In this lossless simplified model, the measured quantity is the time evolution of the backward wave at the probe input, *i.e.*,  $r(t) = L^{-1}[S_{11}(s)(1/s)]$  where  $S_{11}$  is the reflection coefficient at the cable-probe discontinuity,  $s = \sigma + j\omega$  is the Laplace variable,  $L^{-1}$  is the inverse Laplace transform operator, and lower-case and upper-case letters are used to indicate transform pairs.

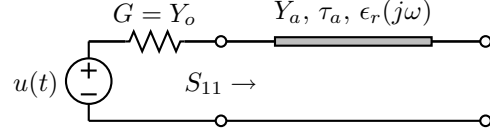


Figure 1: Ideal model of a TDR measurement system.

When the probe is filled by a dielectric with the relative permittivity  $\epsilon_r(s)$ , the  $S_{11}$  function is:

$$S_{11}(s) = \frac{\Gamma + P^2}{1 + \Gamma P^2} \quad (1)$$

where  $\Gamma(s) = (Y_o - Y_a \sqrt{\epsilon_r(s)}) / (Y_o + Y_a \sqrt{\epsilon_r(s)})$  is the partial reflection coefficient at the cable-probe discontinuity and  $P(s) = \exp(-s\tau_a \sqrt{\epsilon_r(s)})$  is the propagation factor along the probe.

The Debye's permittivity model is considered to describe the unknown permittivity:

$$\epsilon_r(s) = \epsilon_\infty + (\epsilon_s - \epsilon_\infty) / (1 + \frac{s}{\omega_{rel}}) \quad (2)$$

where  $\epsilon_\infty$ ,  $\epsilon_s$  and  $\omega_{rel} = 2\pi f_{rel}$  are the model parameters. Therefore, the measurement setup is described by five parameters ( $\epsilon_s$ ,  $\epsilon_\infty$ ,  $\omega_{rel}$ ,  $Y_a$ ,  $\tau_a$ ). To facilitate the analysis, the following normalized quantities are introduced:

$$T = \tau_a \sqrt{\epsilon_\infty} \omega_{rel}, \quad \eta = \epsilon_s / \epsilon_\infty, \quad \mathcal{Y} = Y_a \sqrt{\epsilon_\infty} / Y_o \quad (3)$$

together with the normalized time  $T = t \omega_{rel}$  and complex frequency  $S = s / \omega_{rel}$ . The analysis exploits the decomposition of the normalized reflection coefficient,  $\bar{S}_{11}(S)$ , into a sequence of echoes:

$$\bar{S}_{11}(S) = \bar{\Gamma}(S) + (1 - \bar{\Gamma}^2(S)) \bar{P}^2(S) + (1 - \bar{\Gamma}^2(S)) (-\bar{\Gamma}) \bar{P}^4 + \dots \quad (4)$$

The partial reflection coefficient,  $\bar{\Gamma}(S)$ , and the propagation factor,  $\bar{P}(S)$ , can be expressed as a function of the normalized quantities as follows:

$$\bar{\Gamma}(S) = \frac{1 - \mathcal{Y} \sqrt{\bar{\epsilon}}}{1 + \mathcal{Y} \sqrt{\bar{\epsilon}}} \quad (5)$$

$$\bar{P}(S) = e^{-TS \sqrt{\bar{\epsilon}}}$$

where  $\mathcal{Y} = Y_a \sqrt{\epsilon_\infty} / Y_o$ , and  $\bar{\epsilon} = 1 + (\eta - 1) / (1 + S)$  and  $S = j\Omega$  where  $\Omega$  is the normalized angular frequency.

The first term of equation (4),  $\bar{H}_1(S) = \bar{\Gamma}(S)$ , is the network function relating the incident wave to the

\*Dipartimento di Elettronica, Politecnico di Torino, C.so Duca degli Abruzzi 24, 10129 Torino, Italy, e-mail: patrizia.savi@polito.it

wave reflected by the cable-probe discontinuity. The second term,  $\bar{H}_2(S) = (1 - \bar{\Gamma}^2(S)) \bar{P}^2(S)$ , relates the incident wave to the wave reflected by the probe load and so on. In the time domain, these terms start at  $T = 0, 2T, 4T, \dots$ , and give rise to the echoes forming the observed response, *i.e.*,  $\bar{r}(T) = \bar{r}_1(T) + \bar{r}_2(T) + \dots$ . In order to study the properties of the ideal model responses, it is expedient to focus on the second echo, because it is the simplest term containing information on both the probe-cable discontinuity and on the propagation in the dielectric. The behavior of the second echo is decided by the network functions  $\bar{H}_2(S)$  and, in particular, by the square propagation factor  $\bar{P}^2(S) = \exp(-2TS\sqrt{\bar{\epsilon}})$ . Figure 2a,b shows  $|\bar{P}^2(j\Omega)|$  for  $T = 6, 15, 40$  and  $\eta = 1.5, 3$ . (Panel b is a close-up view of the middle lower part of panel a). For growing  $T$  and  $\eta$  values, the high-frequency magnitude of  $|\bar{P}^2|$  becomes negligibly small and, therefore,  $\bar{H}_2$  becomes a bandlimited function. This bandlimiting effect is due to the imaginary part of  $\bar{\epsilon}(j\Omega)$ , that is responsible for the attenuation constant of  $\bar{P}^2$ :

$$\begin{aligned} \alpha &= -\Re\{j2\Omega T \sqrt{\bar{\epsilon}(j\Omega)}\} = \\ &= -2\Omega T \Im\left\{\sqrt{1 + \frac{\eta-1}{1+j\Omega}}\right\} \end{aligned} \quad (6)$$

The attenuation constant is plotted vs. frequency in Fig. 2c. Every attenuation curve is composed of a quadratic low-frequency part (the constant slope part in the bi-logarithmic scales of Fig. 2c) and by a constant high-frequency part. The constant part arises from the high frequency behavior of  $\Im\{\sqrt{\bar{\epsilon}(j\Omega)}\}$ , that is inversely proportional to  $\Omega$ . The high-frequency asymptotic value of  $\alpha$  is:

$$\lim_{\Omega \rightarrow \infty} \alpha(j\Omega) = \xi = T(\eta - 1) \quad (7)$$

and the asymptotic value of  $|\bar{P}^2|$  is  $\exp(-\xi)$ . For  $\xi = 5$ , the asymptotic value of  $|\bar{P}^2|$  is close to  $6.7 \times 10^{-3}$  and can be considered small. The relation between the  $|\bar{P}^2|$  and  $\alpha$  curves of Fig. 2 is explained by this property. Bandlimited propagation factors are associated to attenuation curves with  $\xi > 5$ , and the propagation factors become small where their attenuation curves overpass the threshold level (see Fig. 2a,b,c).

In the following, we use the term low-attenuation (high-attenuation) to indicate measurement setups and TDR responses characterized by  $\xi > 5$  ( $\xi \leq 5$ ). Measurement setups working in high-attenuation conditions have  $\bar{H}_2$  functions with small high frequency magnitudes. In these conditions, the network functions of the higher order echoes have small high-frequency magnitudes as well, because they include powers of the factor  $\bar{P}^2$ . As a consequence, in high-attenuation conditions, the high-frequency content of the measured TDR waveforms is low and their relation to the high-frequency

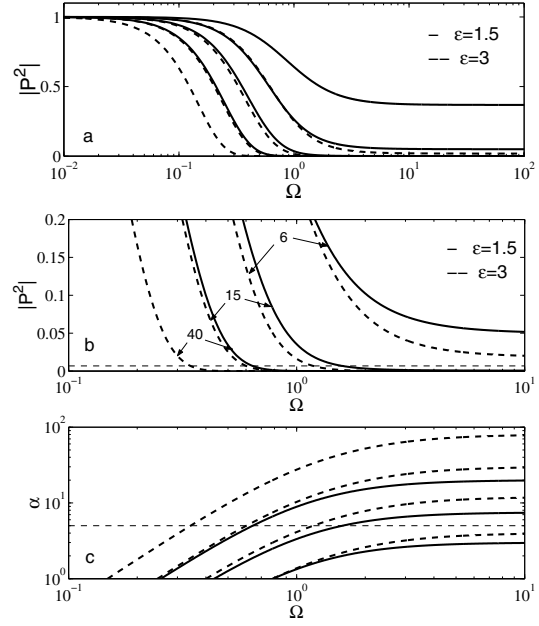


Figure 2: Magnitude of the propagation factor  $P$  (a and b) and attenuation constant  $\alpha$  (c) versus normalized angular frequency  $\Omega$  for  $T = 6, 15, 40$  and  $\epsilon = 1.5, 3$ . Panel b is a close-up view of panel a. The dashed horizontal lines of panel b and c indicate the threshold level  $|\bar{P}^2| = \exp(-5)$  and  $\xi = 5$ , respectively.

permittivity spectrum is expected to be weak. According to this analysis, measurement setup operating in the low-attenuation domain are preferable.

As an example, consider the TDR waveforms corresponding to the low- and high-attenuation frequency responses shown in Fig. 3 for the case  $\epsilon_s = 12$ ,  $\epsilon_\infty = 6$ ,  $f_{rel} = 0.7$  GHz,  $Z_a = \sqrt{\mathcal{L}/\mathcal{C}} = 77 \Omega$ ,  $\tau_a = 0.34$  ns (low-attenuation,  $\xi = 3.7$ ) and  $\tau_a = 1$  ns (high-attenuation,  $\xi = 11$ ). When the wave reflected from the probe end has harmonic components with significant amplitude for frequency larger than  $f_{rel}$  the observed TDR waveforms are of low-attenuation type. This reflection behavior is illustrated in the top panel of Fig. 3, where the solid line curve is the magnitude of the network function of the first echo from the probe end for a low-attenuation case and the dotted straight line correspond to the relaxation frequency (the bandwidth of the instrument source is larger than the relaxation frequency of the dielectric under test). Similarly, when the harmonic components of the wave reflected from the probe end have negligible amplitude for frequency larger than  $f_{rel}$ , the TDR waveforms are of high-attenuation type (dashed curve of the top panel of Fig. 3). The bandwidth of the waveforms of high-attenuation type is therefore inherently limited to  $f_{rel}$ , regardless of the source bandwidth, and these waveforms are scarcely sensitive to the high-frequency parameters of the permittivity. The

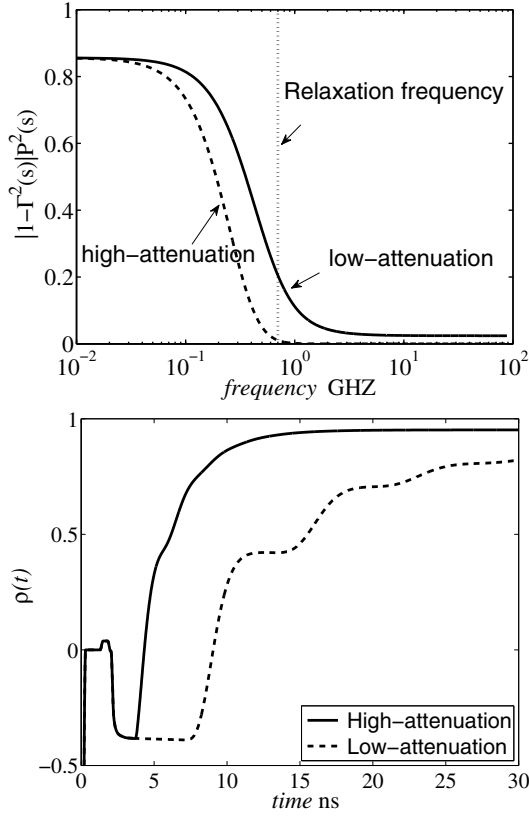


Figure 3: Top panel: magnitude of the network function of the first echo from the probe end for a low-attenuation case (solid line) and an high-attenuation case (dashed line). Bottom panel: TDR waveforms corresponding to the response of the top panel. Dashed line: low-attenuation,  $\tau_a = 0.34$  ns and  $\xi = 3.7$ . Solid line: high-attenuation,  $\tau_a = 1$  ns and  $\xi = 11$ .

two types of waveform can be easily identified because, in the low-attenuation waveform, the rising edge corresponding to the first echo from the probe end is asymmetric and fast, whereas, in the high-attenuation case, the edge is symmetric and slow.

The low-attenuation condition can be expressed in physical parameters as:

$$\xi = \tau_a \omega_{rel} \frac{\epsilon_s - \epsilon_\infty}{\sqrt{\epsilon_\infty}} < 5 \quad (8)$$

or, equivalently, as:

$$2\tau_a \sqrt{\epsilon_\infty} < 10 \epsilon_\infty / \omega_{rel} (\epsilon_s - \epsilon_\infty) \quad (9)$$

where  $2\tau_a \sqrt{\epsilon_\infty}$  is the probe round trip delay. This means that  $2\tau_a \sqrt{\epsilon_\infty}$ , i.e., the probe electrical length, must be limited in order to obtain low-attenuation operation.

The properties of the TDR waveforms pointed out with this analysis yield elementary relations for estimating  $\epsilon_s$  and  $\epsilon_\infty$  directly from the characteristic points of the waveform.

For large  $\xi$  values, elementary relations hold for  $\epsilon_s$  only, which can be estimated as:

$$\epsilon_s \sim \left( \frac{t_b}{2\tau_a} \right)^2 \quad \text{or} \quad \epsilon_s \sim \left[ \frac{Y_a(1+h)}{Y_o(1-h)} \right]^2 \quad (10)$$

where  $t_b$  is the delay of the inflection point of the first rising edge, and  $h$  is the level of the reflection between the first two edges. The second relation is well known, while the first one arises from the properties of the large attenuation condition. For small  $\xi$  values, on the other hand, the rising edges are asymmetric and start at  $2\tau_a \sqrt{\epsilon_\infty}$ . Both  $\epsilon_s$  and  $\epsilon_\infty$  can be estimated by:

$$\begin{aligned} \epsilon_\infty &\sim \left( \frac{t_a}{2\tau_a} \right)^2 \\ \epsilon_s &\sim \left[ \frac{Y_a(1+h)}{Y_o(1-h)} \right]^2 \end{aligned} \quad (11)$$

where  $t_1$  is the delay of the first rising edge.

### 3 RESULTS

The results obtained by using (10,11) (low-level method) has been compared with a method for the permittivity evaluation described in [4] (derivative method). In this method, the permittivity is calculated from the travel time of the TDR signal along the probe (as in the method described in [3]), but the starting point and ending point of the travel time is determined from the apex of the derivative of the waveform of the reflected signal.

The samples were inserted in a coaxial probe terminated on a 50  $\Omega$  load (Maury Microwave Airline, model no. 2653S10, length  $\ell = 10.5$  cm, shield and inner conductor radii 3.5 mm and 1.5 mm, respectively, dc-resistance of inner conductor 9.4 m $\Omega$ /m). Two different instruments were used in order to measure the time-domain response: a Tektronix 1502B reflectometer with rise time  $t_r = 0.3$  ns (horizontal setting 0.1 m per division and a propagation velocity setting of 0.99) and a digitalizing oscilloscope HP54120B with rise time  $t_r = 10$  ps.

The low-frequency permittivity  $\epsilon_s$  obtained with the low-level method (dotted line) and the derivative method (solid line) have then been calculated for a sandy soil with different water content and using the two different measurement setup previously described. The results are shown in Fig. 4, and 5. The permittivity estimated via a parametric inversion approach based on an high-order model [5] is also shown (dashed line).

As it was expected, the values obtained with the three methods are in good agreement. The three methods works better in the case of the HP54120B digitalizing oscilloscope measurement setup due to the better signal to noise ratio of this instrument with respect the Tektronics.

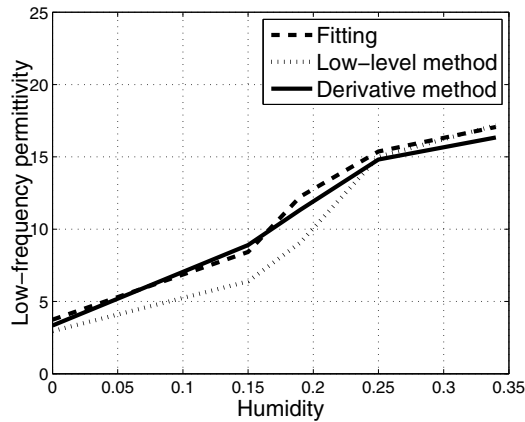


Figure 4: Low-frequency dielectric permittivity for a sandy soil with different water content. Tektronic measurement setup. Comparison between the fitting, the low-level method and the derivative method.

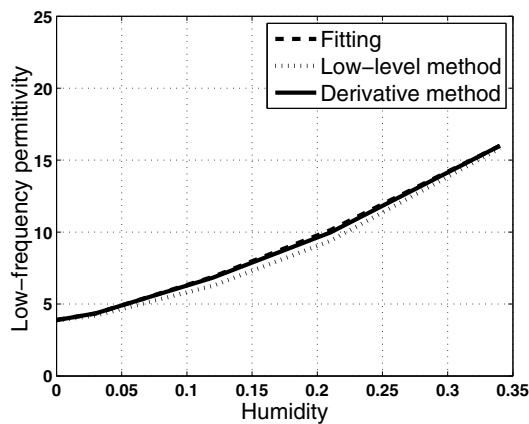


Figure 5: Low-frequency dielectric permittivity for a sandy soil with different water content. HP digitalizing oscilloscope HP54120B measurement setup. Comparison between the fitting, the low-level method and the derivative method.

method based on the travel time of the TDR signal along the probe and with the results obtained with a parametric inversion approach based on an high-order model. When using the digitalizing oscilloscope instead of a standard reflecometer, due to a better signal to noise ratio, the comparison works better.

## References

- [1] Topp, G.C., and P.-A. Ferrè, Water content, in *Methods of soil analysis, Part 4, Physical methods*, SSSA Book, vol.5, edited by J.H. Dane and G.C. Topp, *Soil Sci.Soc. of Am.*, 417-446, Madison, Wis., 2002.
- [2] D.A. Robinson, S.B. Jones, J.M. Wraith, D. Or, and S.P. Friedman, "A Review of Advances in Dielectric and Electrical Conductivity Measurement in Soils Using Time Domain Reflectometry", *Vadose Zone Journal*, Special Section - Advances in Measurement and Monitorin, 2:444-475, 2003.
- [3] G.C. Topp, J.L. Davis, A.P. Annan, "Electromagnetic Determination of Soil Water Content: Measurements in Coaxial Transmission Lines", *Water Resources Research*, vol. 16, no. 3, pp. 574-582, 1980.
- [4] D.A. Robinson, M.G.Schaap, D. Or, S.B. Jones, "On the effective Measurement frequency of time domain Reflectometry in Dispersive and non Conductive Dielectric Materials", *Water Resources Research*, vol. 41, W02007, pp. 1-9, 2005.
- [5] P. Savi, I.A. Maio, "Soil permittivity estimation from TDR measurements:properties and guidelines", *Proc. ICEAA07, International Conference on Electromagnetics in Advanced Applications*, Torino, Italy, Sep. 17-22, 2007.

## 4 CONCLUSIONS

Simple and reliable relations to evaluate the low-frequency permittivity directly from the TDR waveforms are introduced. These formulas are easy to use, and in good agreement with the results obtained with a